Vol. 31(1):1-9 | Ocean and Polar Research | March 2009

Article

An Estimation of Water Structure and Dynamics in the East/Japan Sea Shelf Zone Using Acoustic Tomography

Victor Anatolievich Akulichev*, Vladimir Victorovich Bezotvetnykh, Yury Nikolaevich Morgunov, Yury Alexandrovich Polovinka, and Dmitry Sergeevich Strobykin

V.I. Il'ichev Pacific Oceanological Institute, Far Eastern Branch
Russian Academy of Sciences, Vladivostok 690041, Russia

Abstract : When evaluating acoustic methods for measuring physical parameters in the ocean, economical and technical considerations are paramount. As an indirect method of estimating ocean dynamics, acoustic tomography has advantages over more conventional approaches. It allows the reconstruction of temperature and flow fields from the acoustic impulse time-of-flight measured along the rays propagating from the source to the receiver. However, many problems require complicated and expensive systems. To use the acoustic tomography method to best effect, developing hardware systems with sources and receivers mounted permanently on the sea bottom is crucial. Akulichev et al. presented some experimental results from shallow zones of the World Ocean that served as a motive for developing a multifunction system with acoustic hardware and software. Here we present technical features and the sea test results of the system.

Key words : ocean tomography, ocean thermometry, head-on sounding, multiplex signals, shelf zone

1. Acoustic Tomography Systems and Signal Processing

Tomography systems use multiplex phase-manipulated signals to monitor marine environments. They measure the travel times of impulses propagating along different ray trajectories in a waveguide. By inverting the travel times, one can retrieve temperature and flow fields, and measure tidal and inner wave parameters.

Our system consisted of two transceivers placed 2098 m apart that were connected to the coastal laboratory by cables (Fig. 1). The near transceiver, which was mounted 400 m offshore at a depth of 39 m (1 m from the bottom), consisted of two piezoceramic rings of 1 m diameter. The system transmitted and received acoustic signals in the 366-5000 Hz frequency range. Each transceiver consisted of two hydrophones spaced 3 m apart, with a piezoceramic source of frequency 2500 Hz placed in the center.

The acoustic centers of the hydrophones and source were 35 cm above the bottom. The system contained depth and temperature sensors with 2.5 cm and 0.01°C precision, respectively. A four-core cable was used for remote control and power. The electronic part of the system was separated into two blocks: a coastal and a marine side. The blocks were connected by an analog-to-digital line. The acoustic signals were transmitted in analog form (each channel was transmitted in a separate line), but the temperature and pressure data were sent in digital form. The frequency-modulated digital signals from the sensors were added to the analog signal from the second hydrophone. Remote-control commands were transmitted from the coastal laboratory along the first hydrophone line.

The system was mounted in the acoustic and oceanographic testing ground of the V.I. Il'ichev Pacific Oceanological Institute, FEB RAS, East/Japan Sea shelf zone near Gamov Peninsula. The bottom topography in the experimental area was almost flat, with small depth gradients from 40 to 43 m. The alignment of the system was 173°, which almost coincided with the north-south direction.

Fig. 2 shows a block diagram of the system. In the

*Corresponding author. E-mail : akulich@poi.dvo.ru

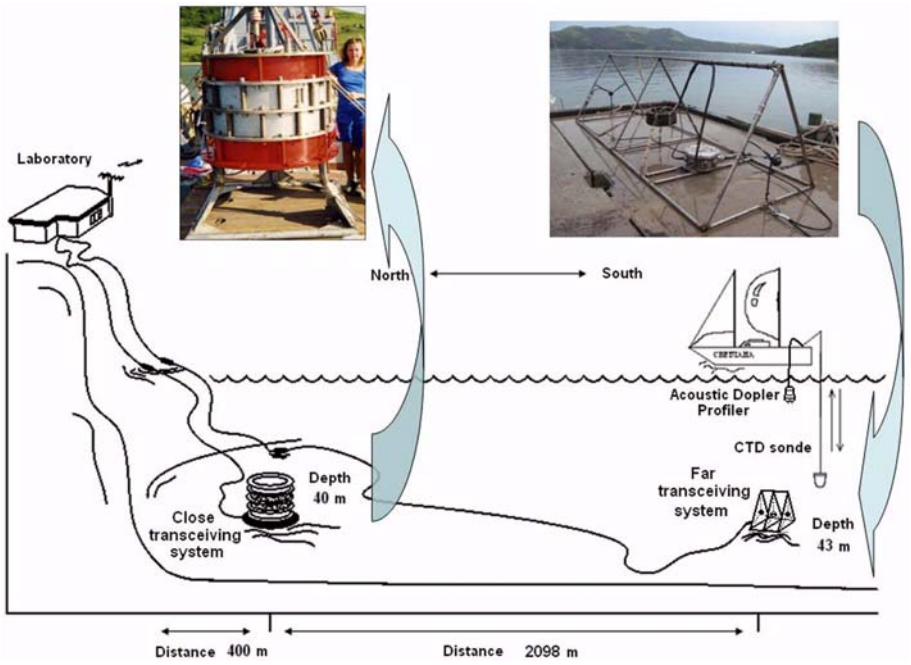

Fig. 1. Schematic of the hardware locations.

pulse characteristic measuring mode, the signals were transmitted from the near system and received by the two hydrophones in the far system. Test signals (phase-manipulated signals of 511 symbols, with four carrier frequency periods per symbol) were injected into the source. Signals and data from the depth and temperature sensors were amplified and transmitted to the analog-to-digital converter located at the coastal laboratory for registration and analysis.

In the head-on sounding mode for flow velocity measurement, the same multiplex signals were used. The signals were synchronized by the common-timing system and transmitted simultaneously from the transducers of both systems. They were then received by the transducers of both systems and transmitted to the analog-to-digital converter located at the coastal laboratory.

The procedures for signal processing were as follows. The cross-correlation function of the received and transmitted signals was

$$K_{ss_0}(\vec{r},\vec{r}_0,t,t_0)=\frac{1}{(2\pi)^2}\int_{-\infty}^{\infty}|S_0(\omega)|^2\cdot G(\omega,\vec{r},\vec{r}_0)\cdot e^{i\omega(t-t_0)}d\omega$$

where $S_0(\omega)=\int_{-\infty}^{\infty}s_0(t)\cdot e^{-i\omega t}dt$ was the Fourier spectrum of the transmitted signal, $G(\omega,\vec{r},\vec{r}_0)=\Sigma_{j=1}^{N}A_j(\vec{r})\cdot e^{-i\omega t_j(\vec{r})}$ was the Green's function in the ray representation, N was the number of rays reaching the receiver, and $t_j(\vec{r})$ and $A_j(\vec{r})$ were the time and amplitude of the signals, respectively, for the i-th ray propagating from the source to the receiver at $\vec{r}$. From these equations, we obtained the pulse characteristics or travel times of the acoustic energy propagating along different ray trajectories in the waveguide. As shown below, the measured data were then used to estimate the dynamics of the water.

2. Sea Experiment Data

The acoustic tomography method uses complex phase-manipulated signals, deriving cross-correlation functions by comparing the received and transmitted signals. Adjusting to the correct frequency range and signal parameters allowed us to select individual rays by their travel times. This travel time information was then used to estimate the speed of acoustic ray propagation along different trajectories, and hence the temperature values in different layers. We made measurements monthly from 2005 to 2006 along an acoustic path of 2098 m. Each measurement continued for 72 hours (3 days). In summer, a research vehicle anchored at the receiving point measured vertical profiles of temperature and salinity every hour.

Fig. 3 shows the typical pulse characteristics over a month. We can see some regular patterns by examining the pulse characteristics.

1. The experimental conditions were such that we could identify up to nine rays propagating between the source and the receiver along different trajectories.

2. From November to April, a pulse formed, with the

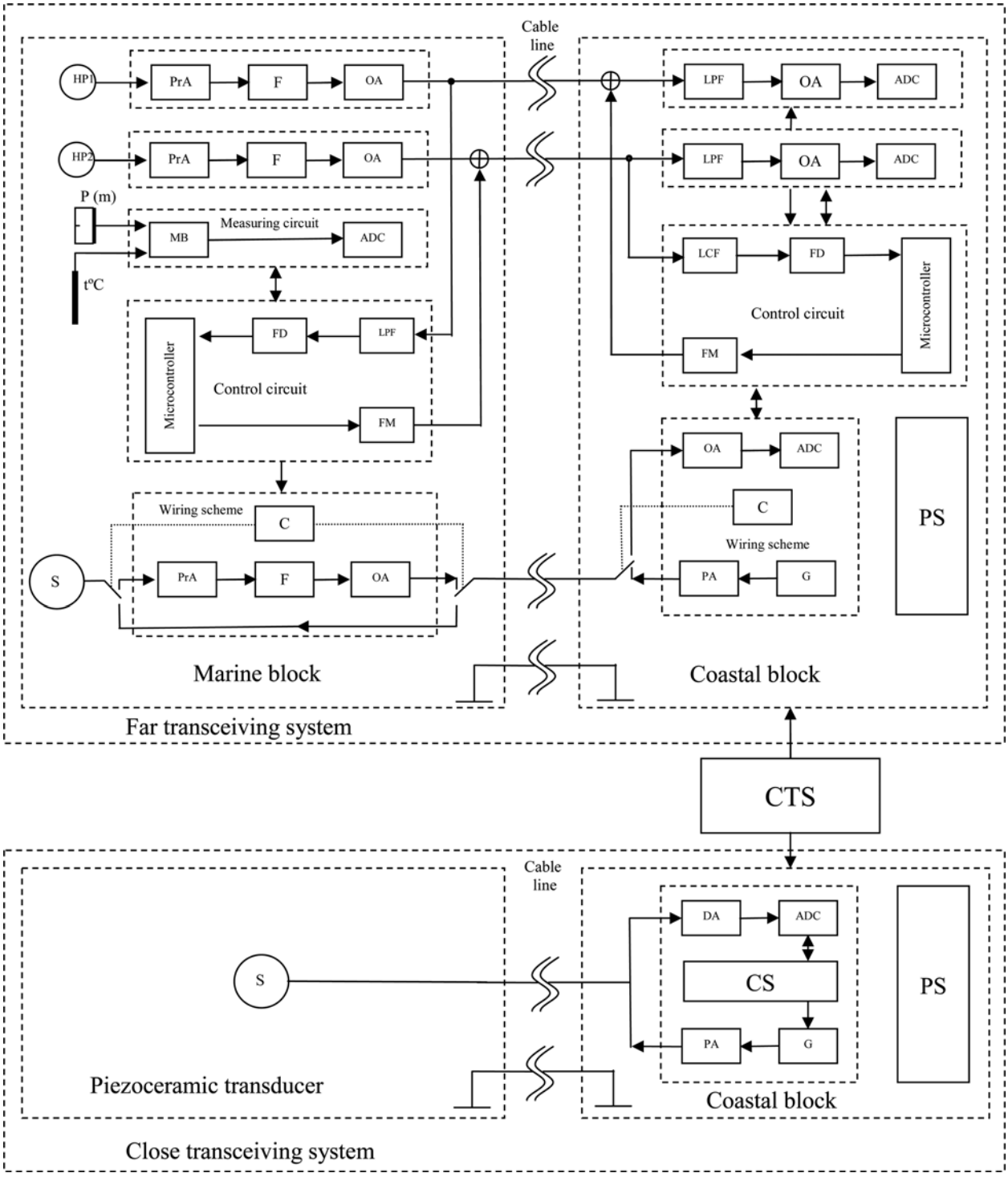

Fig. 2. Block diagram of the hardware and software: (HP) hydrophone, (PrA) preamplifier, (F) filter, (OA) operational amplifier, (ADC) analog-to-digital converter, (S) source, (PA) power amplifier, (CTS) common-timing system, (PS) power supply, (MB) measuring bridge, (C) commutator, (LPF) low-pass filter, (FD) frequency demodulator, (LCF) low-cut filter, (FM) frequency modulator, (G) generator, (DA) differential amplifier, and (CS) control system.

rays reflecting from one to nine times between the surface and the bottom. This was because in the water column, the sound speed was approximately constant with depth, and the rays only reflected, without refracting. The pulse

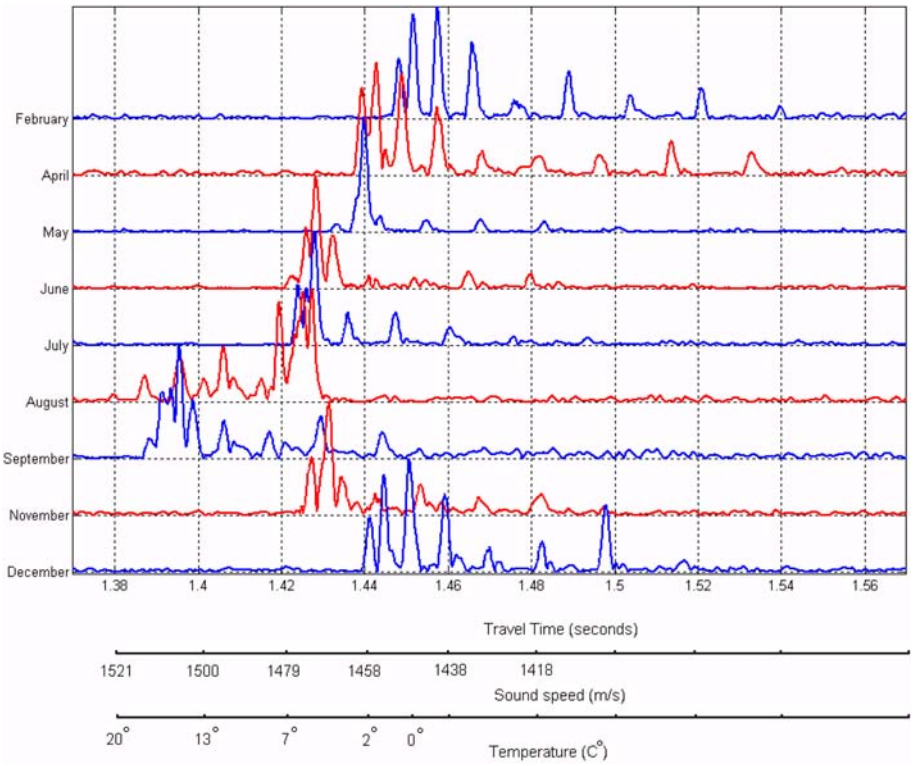

Fig. 3. Pulse characteristics of the waveguide normalized by amplitude, as measured in the experimental region from 2005 to 2006.

intervals were similar for all months, but the impulse responses shifted slightly over time, depending on the phase velocities. The temperature was calculated from the phase velocity using experimental equations such as those of Del Grosso'. The experimental geometry was such that the phase and group velocities of the first pulse were approximately equal, and the temperature could be calculated using this relationship (Fig. 3).

3. In summer, as the upper layer warmed up, small-angle rays began to refract. In addition, rays of no reflection appeared between the first and second pulses. The ultimate temperature in the waveguide could be estimated from the group velocity of the first arrival.

4. In August, cold tidal water intruded into the sea bottom, and a near-bottom sound channel appeared. Under this condition, small-angle rays were trapped, with a minimum phase velocity equal to the group velocity. Referring to Fig. 3, we can see that the late-arriving ray had a velocity of 1475 m/s. Hence, the temperature in the near-bottom layer was approximately 3°C. The temperature of the entire water column could be calculated from the group velocity of the first arrival, which was approximately 20°C in this case.

As an example, we analyzed results from data measured in August and February. The hydrological conditions in August were characterized by periodic semidiurnal temperature field variations, which were related to the cold water coming into the near-bottom layer when the tidal front passed (Fig. 4a).

Fig. 4b shows the periods of the arrival variations recorded for a given acoustic path in August. The data in Fig. 4b and 4c are distributions of the normalized amplitudes as a function of travel time. Evidently, the late arrival time of the acoustic rays correlated most clearly with the thermal changes in the bottom layer. As cold water moved into the source-receiver acoustic path, a near-bottom sound channel formed, causing rays of minimum propagation loss, with small slide angles and sound velocities. Under these conditions, the traveled distance was approximately equal to that of the linear path between the source and receiver. The sound speed and temperature (about 5°C) of the near-bottom layer could be calculated by the measured travel time of the late-arriving ray.

When warm water layers moved downward at low tide, the width of the near-bottom sound channel decreased. This situation caused the acoustic energy to disperse into the upper part of the waveguide. In addition, more intense

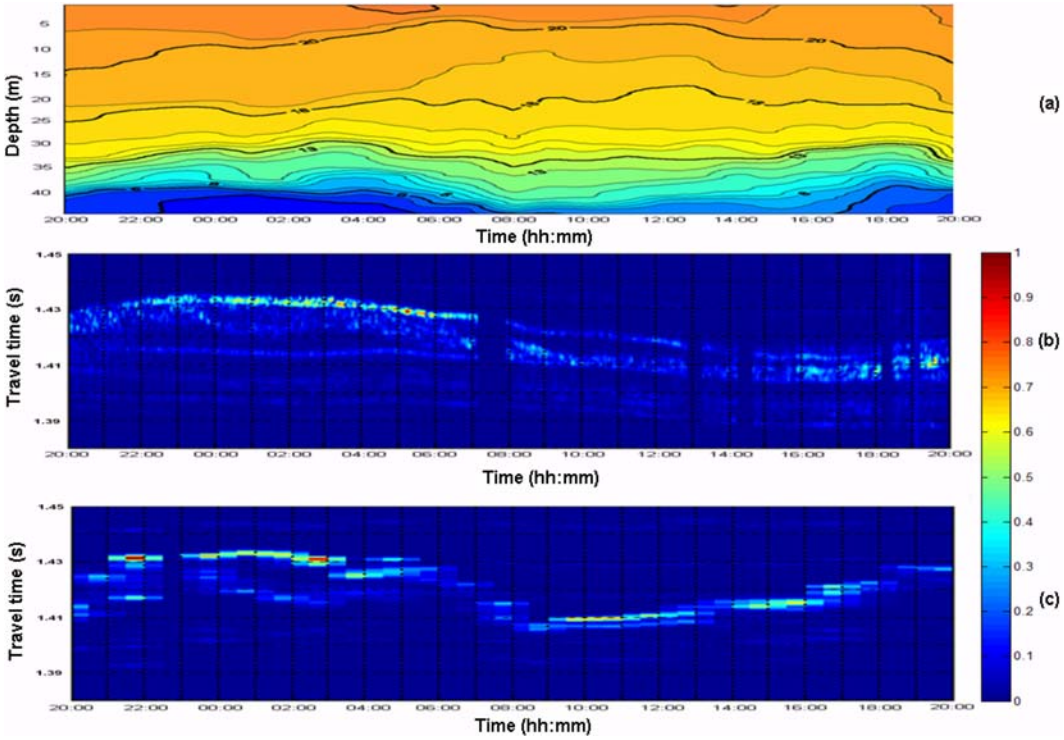

Fig. 4. (a) Dependence of the water temperature on time at different depths. (b) Observed and (c) measured variations of the waveguide pulse characteristics in August 2005.

rays with higher grazing angles and group velocities had arrived earlier. When the near-bottom sound channel disappeared completely (from 08:00 to 17:00 in Fig. 4a), energy dispersed into the earlier arriving rays. In this case, to calculate the phase velocity of each pulse, we had to consider the number of reflections in the waveguide to obtain the effective distance along the ray.

For a more complete analysis of ray arrivals, we used an acoustic model based on ray theory (Porter and Bucker 1987). Fig. 4c depicts the pulse characteristics computed using this model. The computed and measured data (Fig. 4b and 4c) closely agree. Evidently, both the amplitudes obtained experimentally and the time-of-flight of the sound impulses propagating along different ray trajectories were in close agreement with the theoretical calculations. In future work, this model may be employed for a more accurate solution of temperature field reconstruction problems in shallow water areas.

On closer examination of the case when cold water came into the bottom layer, we saw that the late-arriving patterns occurred over an interval of approximately 15 minutes (Fig. 5a). The ADCP (Acoustic Doppler Current Profiler) records verified that the phenomenon was caused by intensive internal wave passage. The ADCP, which was placed 320 m away from the receiving system, measured both water density and three-dimensional currents. The time difference for internal waves arriving at the receiving system and ADCP was approximately 19 minutes. The propagation speed of the waves was approximately 28 cm/s. This result implied that using the tomography system to obtain the parameters of internal waves remotely should be possible.

The water column in February 2006 was so well mixed that sound speeds and temperatures were nearly constant from the surface to the bottom. Fig. 6b shows the (computed) tide level variation, together with the temperature contours during the experiment. This condition caused seven rays to arrive at the receiving point due to one to seven reflections within the water column (Fig. 6a). We can clearly identify the seven ray arrivals, which varied over 12 hours. The travel time variations in the modeled and measured data showed close agreement, as shown in Fig. 6c.

When studying hydro-physical processes by acoustic tomography methods in shallow waters, considering the effect of depth changes when a tidal wave passes through the experiment area is crucial. The direct measurements of tide levels with oceanographic instruments inevitably contain much high-frequency noise. Attempts to separate a tidal component from the acoustic signals often (in the summer-autumn period) led to some error because the

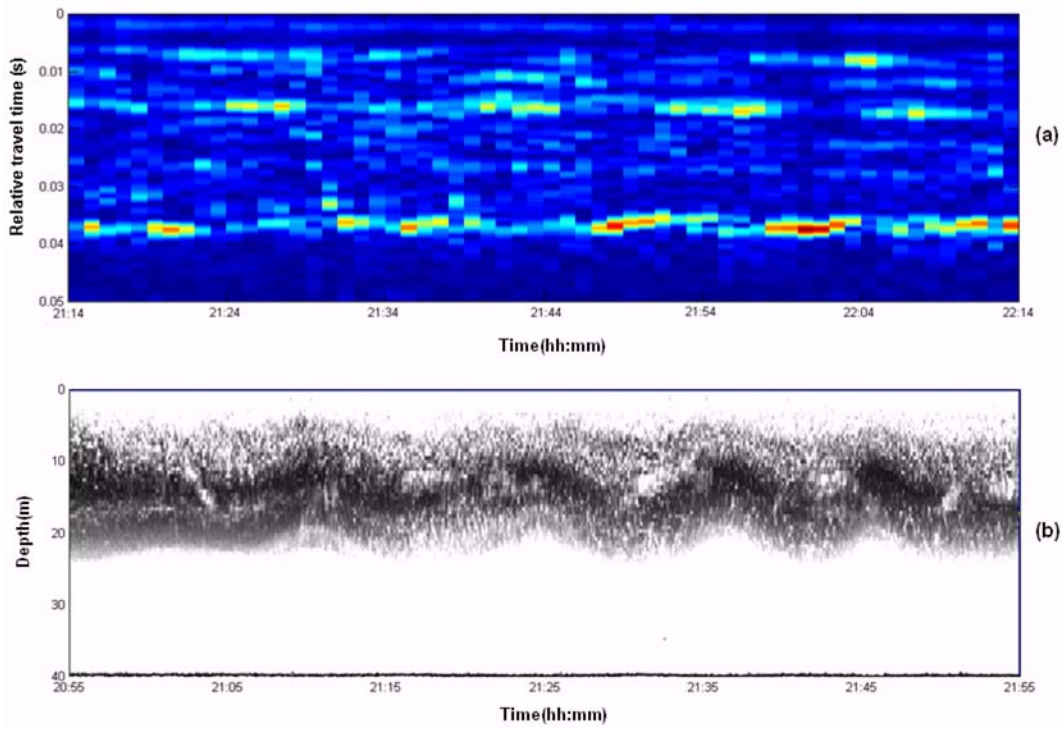

Fig. 5. (a) Waveguide pulse characteristics and (b) ADCP data showing the density variability of the water in September 2004.

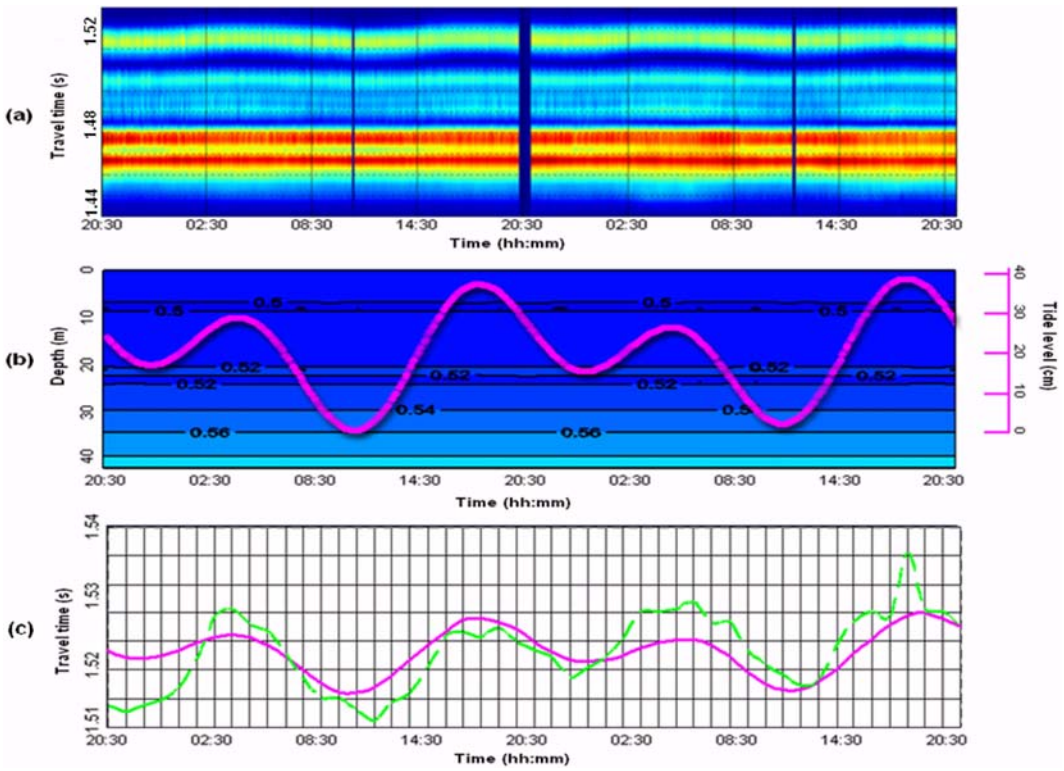

Fig. 6. (a) Waveguide pulse characteristic variations, (b) tidal variation with time as calculated in Harris (2000) and isotherms, and (c) travel time variations of the seventh arrival (dotted and solid lines show experimental and theoretical data, respectively).

tidal waves may have dominated the influence of the temperature variations on the stationary path. That is, this occurred because the internal full tide arrived at the measuring systems later than the sea depth change, owing to its slower propagation along the shelf.

We also examined the possibility of using the calculated tidal rise data (Harris 2000) to reconstruct the temperature fields in a waveguide. We selected the period from 28 February to 2 March 2006 when calm-sea weather conditions occurred. The sound speed and temperature of the water column was almost constant from the surface to the bottom. The tide level (computed) variation together with the temperature contours are shown in Fig. 6b.

From Fig. 6b and 6c, we can see that the maximum-minimum values of the travel time along the ray corresponded to the maximum-minimum water levels in the full-tide and tide stages, respectively. Referring to Fig. 6c, we calculated the travel time along the ray of the tidal level variations, where the travel time was computed using the ray method acoustic model (Porter 2002). According to the calculated tide-level data (Fig. 6b), the depth varied in 0.1 m steps. The simulation results were in close agreement with the experimental time variations of a pulse traveling along the ray induced by the full tide. Noticeable variations occurred with periods of 2 to 3 hours in the observed dependence, which were likely due to the seiches (stationary waves) caused by the full tides. Hence, we demonstrated that studies involving high-accuracy numerical simulations should consider the influence of tide variations on the sea surface level.

In October 2007, the focus of the experiment was to test the feasibility of the tomography system for estimating currents. One synchronous head-on transmission of the acoustic signals occurred every minute. For each propagation direction, the received and transmitted signals gave the cross-correlation function. The maxima corresponded to the travel times of acoustic rays propagating to the reception point along different trajectories. We measured the travel times of the n-th impulse, t_n^- and t_n^+, which corresponded to the propagation of acoustic signals against and along the flow, respectively. Furthermore, we also calculated the sum $S_n = t_n^+ + t_n^-$ and difference $\Delta t_n = t_n^- - t_n^+$ of travel times, the components of flow velocity $V_n = \Delta t_n \cdot c_n^2/2$ along the path of length r traveled by the n-th impulse, and the velocity of signal propagation in the path, $c_n = 2r/S_n$.

Fig. 8a and 8b show the pulse characteristics measured using a head-on sounding method and ray diagrams, respectively. The first five arrivals passed the path along different ray trajectories and different numbers of reflections in the waveguide. The sixth arrival with the highest amplitude was due to a group of rays propagating in a cold-water near-bottom sound channel. A comparison of the pulse characteristics showed that the main patterns of the

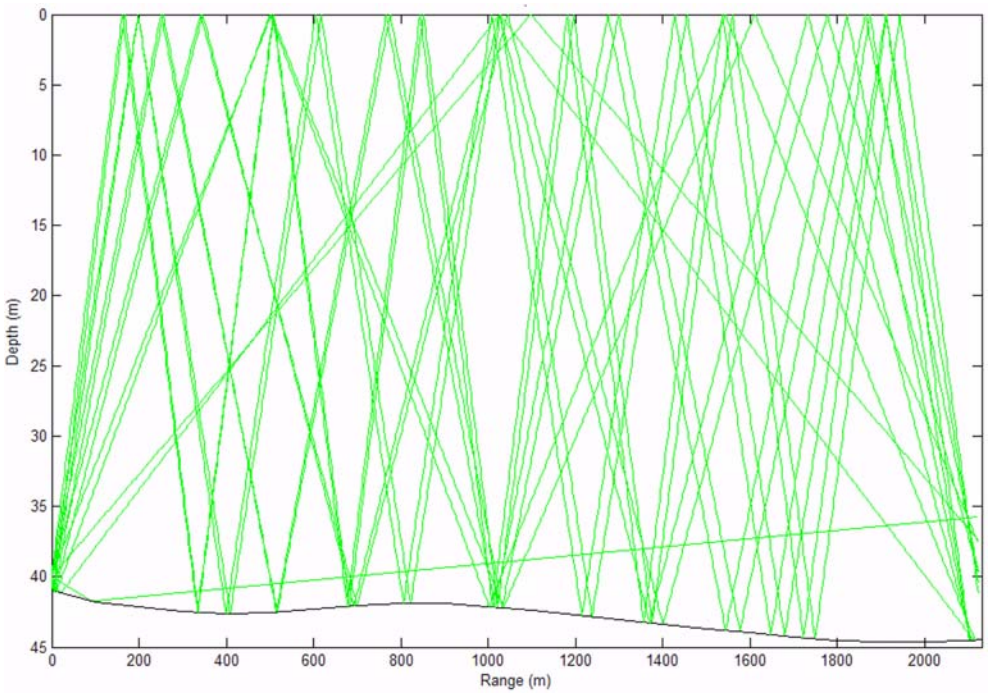

Fig. 7. Ray diagrams for February 2006 hydrological conditions (Fig. 6b).

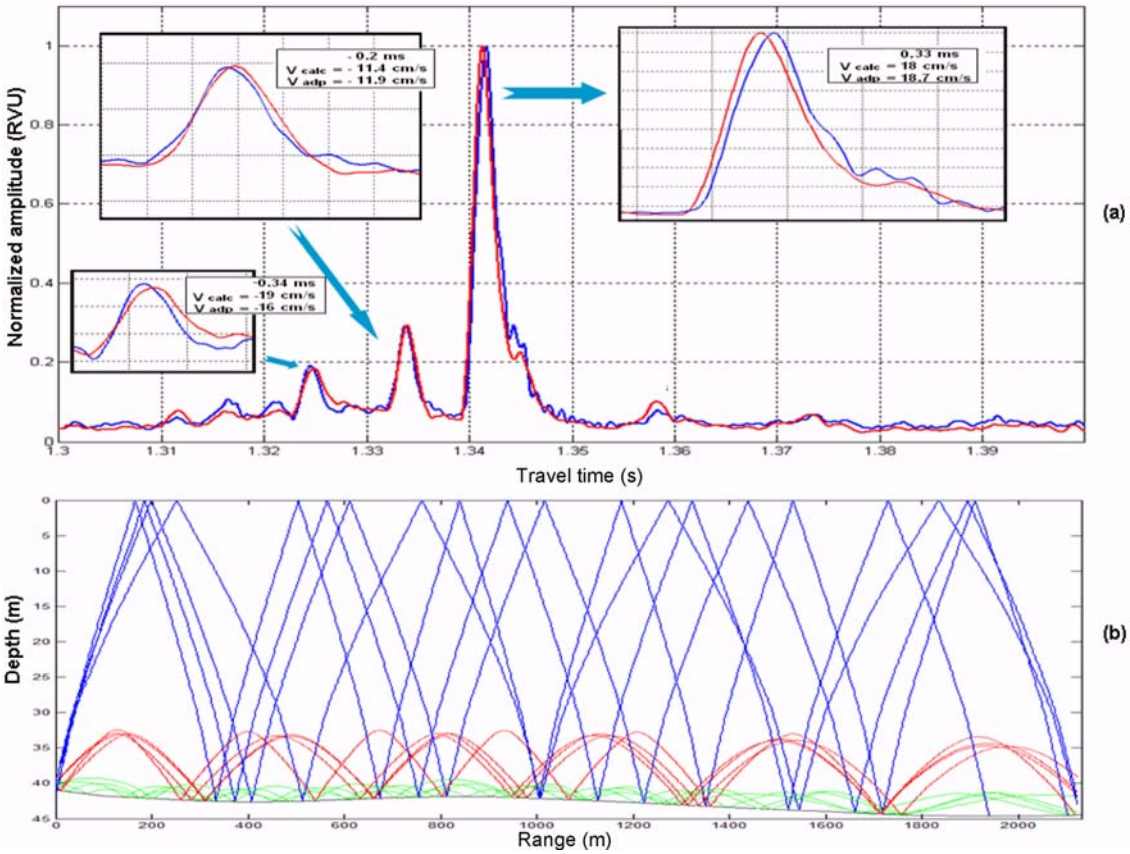

Fig. 8. (a) Pulse characteristics measured using the head-on sounding method. The blue curve shows the direction from the close system to the far system, while the red curve shows the direction from the far system to the close system. (b) Ray diagrams for October 2007 hydrological conditions.

acoustic fields were identical whether the rays propagated along or against the flow. This fact approximately verified the reciprocity principle in acoustic energy propagation. Currents were computed for the fourth, fifth, and sixth impulses because these impulses had sharp peaks against the noise. The computed currents revealed that the flow direction in the near-bottom layer was away from the coast, while that integrated over a whole water column was toward the coast (Fig. 8a). This was in agreement with the ADCP data from that period.

3. Conclusions

We described the main features of the tomography system developed by the POI FEB RAS for estimating shallow water dynamics. We demonstrated that acoustic signals from the tomography system might be used to reconstruct temperature and current fields with tolerable error bounds. The system was able to study dynamic processes on timescales from a few minutes to a year or more.

Acknowledgements

This study was presented at the 3rd KORDI-POI workshop, South Sea Institute, KORDI, 2007. We thank A.N. Serebriany and P.G. Kushnir for providing the hydrophysical data. We also wish to acknowledge the helpful comments of the OPR reviewers.

References

Akulichev VA, Bezotvetnykh VV, Voitenko EA, Kamenev SI, Leont'ev AP, Morgunov YuN (2004) Acoustic remote sensing of currents at the shelf of the Sea of Japan. Acoust Phys **50**(5):493-495

Akulichev VA, Bezotvetnykh VV, Kamenev SI, Kuz'min EV, Morgunov YuN, Nuzhdenko AV, Penkin SI (2000) Acoustohydrophysical complex for marine tomographic research. Instrum Exp Tech **43**(6):829-832

Akulichev VA, Bezotvetnykh VV, Kamenev SI, Kuz'min EV, Morgunov YuN, Nuzhdenko AV (2002) Acoustic tomography of dynamic processes in a sea shelf zone with the use of complex signals. Acoust Phys **48**(1):1-7

Harris M (2000) Tidecomp world wide predictor. V. 7.03. http://www.pongolin.co.nz

Porter MB, Bucker HP (1987) Gaussian beam tracing for computing ocean acoustic fields. J Acoust Soc Amer **82**: 1349-1359

Porter MB (2002) Acoustic Toolbox. Underwater Acoustic Propagation Modeling Software. http://oalib.hlsresearch.com/Modes/AcousticsToolbox

Received Apr. 30, 2008
Accepted Jul. 2, 2008